

Science Meets Technology with Advanced Optical Metrology




Access in-depth information on methods and applications in the R&D field of optical metrology through free to access article digests of recent peer-reviewed publications and more.

Discover advancedopticalmetrology.com now!

OLYMPUS

WILEY

Advanced cryo-tomography workflow developments – correlative microscopy, milling automation and cryo-lift-out

JAKUB KUBA*, JOHN MITCHELS*, MILOŠ HOVORKA*, PHILIPP ERDMANN† , LUKÁŠ BERKA*, ROBERT KIRMSE‡ , JULIA KÖNIG‡, JAN DE BOCK§, BERNHARD GOETZE|| & ALEXANDER RIGORT†, || 

*Thermo Fisher Scientific Brno s.r.o., Brno, Czech Republic

†Department of Molecular Structural Biology, Max Planck Institute of Biochemistry, Martinsried, Germany

‡Leica Microsystems GmbH, Vienna, Austria

§Leica Microsystems CMS GmbH, Mannheim, Germany

||Thermo Fisher Scientific, FEI Deutschland GmbH, Planegg, Germany

Key words. Cryo-CLEM, cryo-electron, cryo-ET, cryo-FIB, cryo-FIB/SEM, cryo-focused ion beam, cryo-lift-out, cryo-LM, electron-tomography, FIB/SEM tomography, focused ion beam, lift-out, tomography workflow.

Summary

Cryo-electron tomography (cryo-ET) is a groundbreaking technology for 3D visualisation and analysis of biomolecules in the context of cellular structures. It allows structural investigations of single proteins as well as their spatial arrangements within the cell. Cryo-tomograms provide a snapshot of the complex, heterogeneous and transient subcellular environment. Due to the excellent structure preservation in amorphous ice, it is possible to study interactions and spatial relationships of proteins in their native state without interference caused by chemical fixatives or contrasting agents. With the introduction of focused ion beam (FIB) technology, the preparation of cellular samples for electron tomography has become much easier and faster. The latest generation of integrated FIB and scanning electron microscopy (SEM) instruments (dual beam microscopes), specifically designed for cryo-applications, provides advances in automation, imaging and the preparation of high-pressure frozen bulk samples using cryo-lift-out technology. In addition, correlative cryo-fluorescence microscopy provides cellular targeting information through integrated software and hardware interfaces. The rapid advances, based on the combination of correlative cryo-microscopy, cryo-FIB and cryo-ET, have already led to a wealth of new insights into cellular processes and provided new 3D image data of the cell. Here we introduce our recent

developments within the cryo-tomography workflow, and we discuss the challenges that lie ahead.

Introduction

Cells are the functional units of all organisms; understanding how they work can help us to unravel the fundamental processes underpinning life itself. Cryo-techniques for electron microscopy (EM) allow to rapidly freeze and preserve cellular samples in a close-to-native, fully hydrated state (Wagner *et al.*, 2017; Plitzko & Baumeister, 2019). The freezing, or so-called vitrification process, is so fast that liquid water forms amorphous (non-crystalline) ice, thus avoiding the damage caused by the formation of crystals typical for slower freezing rates (Brüggeller & Mayer, 1980; Dubochet & McDowell, 1981; Dubochet *et al.*, 1988). Before a vitrified cell can be examined by electron tomography, the target site within the cell must be localised first, followed by the preparation of a thin section containing the target. Recent advances in cryo-FIB-based sample preparation have enabled the preparation of such site-specific thin sections (called cryo-lamellae) from vitrified cells (Marko *et al.*, 2007; Rigort *et al.*, 2012). Essentially, cryo-lamellae provide snapshots of functional cellular environments whose supramolecular architecture can be studied *in situ* at high resolution and in 3D by electron tomography (Mahamid *et al.*, 2016; Guo *et al.*, 2018; Mosalaganti *et al.*, 2018; Albert *et al.*, 2020). This allows structural investigations of biomolecules in the context of the corresponding cellular structures. Studying the molecular machinery of cells with cryo-ET requires a comprehensive workflow covering all steps from sample preparation and vitrification through cryo-light microscopy (cryo-LM), sample thinning by cryo-FIB and

Correspondence to: Alexander Rigort, Max Planck Institute of Biochemistry, Department of Molecular Structural Biology, 82152 Martinsried, Germany. Tel: +49 89 8578-2620; e-mail: rigort@biochem.mpg.de

Robert Kirmse, Leica Microsystems GmbH, Vienna, Austria. E-mail: robert.kirmse@leica-microsystems.com

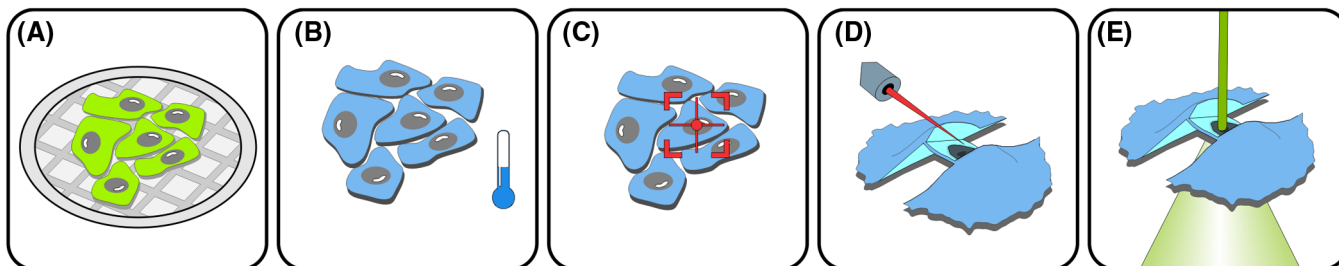


Fig. 1. Schematic illustration of the cryo-ET workflow. (A) Cultured cells on an EM grid. (B) The grid with the cells is frozen rapidly to avoid damage caused by crystallisation. (C) Vitrified cells containing fluorescently labelled structures are identified in a cryo-light microscope. (D) Positions of labelled cells are retrieved in a cryo-FIB/SEM, in which a thin lamella is created by milling away material above and below the feature of interest. (E) The lamella is transferred to a cryo-TEM, where a tomographic image series is acquired.

3D data acquisition in the cryo-transmission electron microscope (cryo-TEM), including safe sample transfers between the individual steps (Fig. 1).

Cryo-lamella preparation often begins with correlative microscopy, where image and coordinate information from fluorescently labelled cellular features is obtained. This is particularly important if such a feature is transient or rare within the cell (e.g. the centrosome), or when it is relevant to check if a certain phenotype is present at all. Here, cryo-correlative light and electron microscopy (cryo-CLEM) can provide the necessary information for localisation (Kaufmann *et al.*, 2014; Schorb & Briggs, 2014; Wolff *et al.*, 2016). As samples in cryo-CLEM are frozen, the fluorescently labelled proteins remain in place, and can be retrieved and correlated later in the cryo-FIB microscope. In addition, cryo-LM provides information about sample quality and therefore helps the decision if a sample is worth investing in time for further processing within the workflow. Cryo-fluorescence imaging is performed in a light microscope, which is equipped with a cryo-stage system that allows imaging samples under cryogenic conditions (Sartori *et al.*, 2007; Schwartz *et al.*, 2007; van Driel *et al.*, 2009; Schorb *et al.*, 2017).

Following localisation, a dual beam cryo-FIB/scanning electron microscope (cryo-FIB/SEM; Fig. 2) is used for thinning the frozen cellular samples to the required thicknesses for cryo-TEM investigations (typically not much more than 200 nm). This is because most cells are too thick to be studied intact by cryo-TEM. In contrast to cryo-ultramicrotomy, a cryo-FIB ablates the sample with a beam of Gallium ions (Fig. 3), thereby leaving the vitrified sample unaffected by compression forces allowing a highly site-specific targeted preparation. The Gallium ions have a high mass and can therefore remove surface layer atoms via sputtering processes (Fig. 3B). Precise milling with the ion beam generates a thin and electron-transparent lamella from a cell by removing cellular material above and below a target region (Rigort & Plitzko, 2015; Schaffer *et al.*, 2015). The SEM provides visual control over the FIB milling process, permitting the creation of cryo-lamellae as thin as 100–200 nm. After cryo-FIB milling, thin cryo-lamellae are

transferred to the cryo-TEM, where a tomographic image series is acquired as the lamella is tilted incrementally. Finally, the images are combined computationally to reconstruct a 3D tomogram of the cellular interior. From the 3D tomographic volume, higher resolution structures of particles (i.e. proteins or protein complexes) can be obtained by averaging out noise in a process termed sub-tomogram averaging (Wan & Briggs, 2016; Zhang, 2019). Conceptually, the procedure compares to single particle analysis, yielding higher resolution structures of the macromolecules detected *in situ*. In the following we introduce new developments for cryo-CLEM and cryo-FIB and discuss their impact for the cryo-tomography workflow.

Correlative cryo-fluorescence microscopy

Locating a structure of interest and preparing a lamella containing this structure is exceedingly difficult in the vast complexity of the cellular environment. Even more so, considering that in a cryo-FIB/SEM only the surface view of a sample is accessible to decide upon the position of the milling windows. Imaging frozen samples by cryo-LM offers the additional benefit of locating the structures of interest very efficiently (Briegleb *et al.*, 2010). Moreover, without exposing the sample to electron beam radiation. Utilising standard fluorescent labelling protocols (e.g. transgenically encoded or lipophilic dyes) target structures in cells can be made selectively visible by fluorescence. Specific cells can be identified, containing the structure of interest for subsequent detailed investigation by cryo-EM. Several scientific setups of cryo-light microscopes are existing, mainly based on standard light microscopes using custom made cryo-sample chambers in combination with long working distance objectives to avoid damages to the optics by the deep temperatures, but limiting the effective resolution (Sartori *et al.*, 2007; Schwartz *et al.*, 2007; van Driel *et al.*, 2009; Rigort *et al.*, 2010). To date, also a few integrated cryo-LM-EM systems have been reported (Faas *et al.*, 2013; Gorelick *et al.*, 2019). Yet, only few commercial systems are available, for example standard upright microscopes with a cryo-stage by Linkam (van Driel *et al.*, 2009; Koning *et al.*, 2014) and

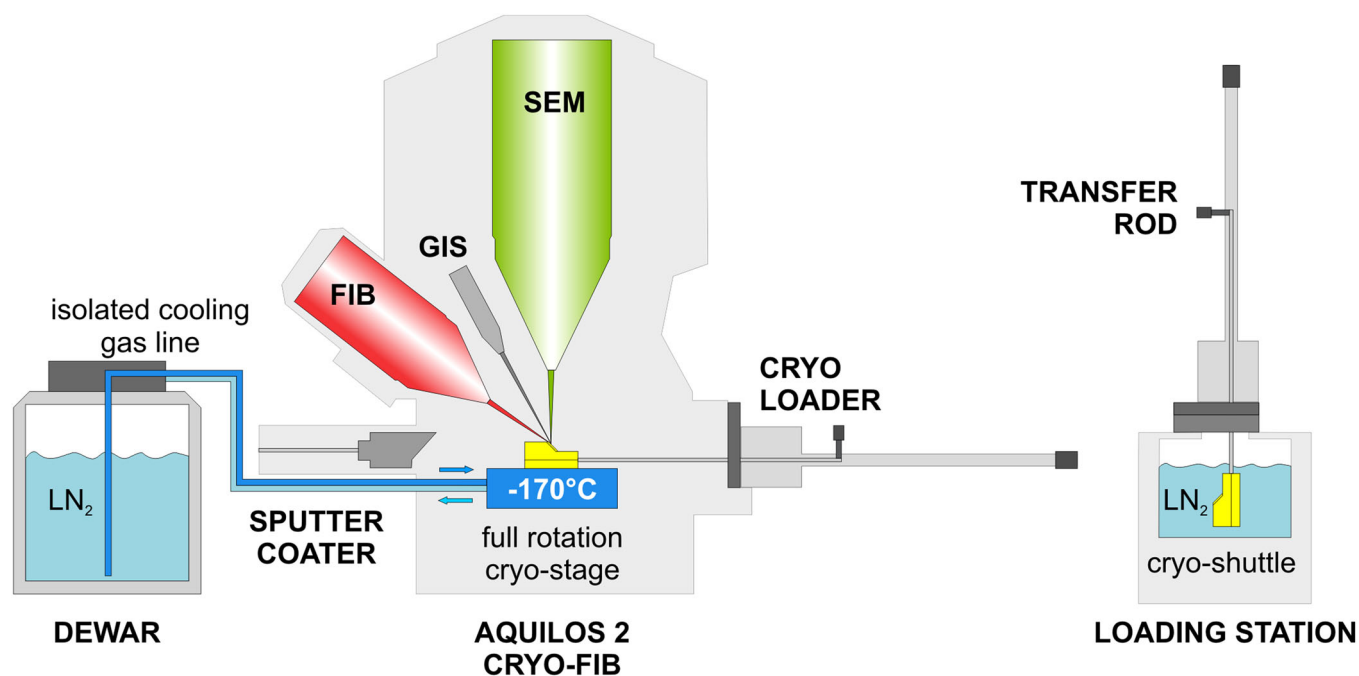


Fig. 2. Cryo-FIB/SEM with associated hardware components. Two EM grids with vitrified samples are loaded into a cryo-shuttle in an external loading station and then transferred under vacuum to the microscope via a transfer rod and an air lock ('cryo-loader'). Inside the microscope, the sample is loaded onto a cryo-stage, which keeps the sample below -170°C by a continuous flow of cold nitrogen gas. The nitrogen gas used for cooling is cooled down via a heat exchanger located in a dewar on the left side of the instrument. The cryo-stage can be moved, rotated and tilted to ensure the accessibility of the sample to the beams (and also to the gas injection system (GIS) and the sputter coater).

a complete system including a dedicated cryo-objective and transfer shuttle provided by Leica Microsystems (Schorb *et al.*, 2017).

With the availability of camera-based widefield or confocal systems, the most suitable technique for a given application can be selected to achieve an optimal cost/needs and effort balance. Whereas confocal microscopes provide a better resolution, in particular along the z -axis, camera-based setups are more sensitive, faster in image acquisition and less cost intensive. Owing to its different illumination principle, widefield acquisition shows a system inherent haze, as out-of-focus light is contributing to the resulting image, since no confocal pinhole is present. This is particularly disturbing as structures of interest must be identified precisely for subsequent EM steps. Fortunately, this phenomenon can be overcome by computational clearing methods (Reymann, 2018; Schumacher & Bertrand, 2019), which can be also applied under cryo-conditions (Fig. 4). This results in a significantly improved image quality revealing the actual image information for subsequent quantification and targeting. As demonstrated in Figure 4, applying deconvolution methods to cryo-imaging can improve the attainable image quality. In confocal microscopy, computational clearing can be utilised for improving the resolution in all dimensions (Fig. 4A'); this is especially true, when considering that current commercial systems are still bound to non-immersion optics for cryo-imaging. So far, only a few exper-

imental cryo-immersion approaches have been reported (Le Gros *et al.*, 2009; Nahmani *et al.*, 2017; Faoro *et al.*, 2018). In summary, both microscopy methods – confocal and widefield – offer unique benefits depending on workflow and user needs.

New developments facilitating correlative data and sample transfer steps

As cryogenic workflows include steps that bear the risk of sample damage or loss of correlation information, any development that facilitates or reduces these steps increases the likelihood that meaningful scientific results can be obtained. We have therefore developed improvements in data and sample transfer, which now allows a closer link between the cryo-light microscope and the cryo-FIB. During cryo-LM acquisition, identified target sites can be interactively marked in the cryo-light microscope software. Their coordinates are later transferred together with the sample to the cryo-FIB software where the exact locations are retrieved (Fig. 5). Importing the cryo-LM data within the cryo-FIB software at the push of a button accelerates steps such as conversion, superimposition and alignment that were previously rather time-consuming. Beside the common software interface, a dual-purpose cryo-holder (Fig. 5A) has been developed, which can be utilised in both instruments. The holder eliminates an otherwise necessary additional sample

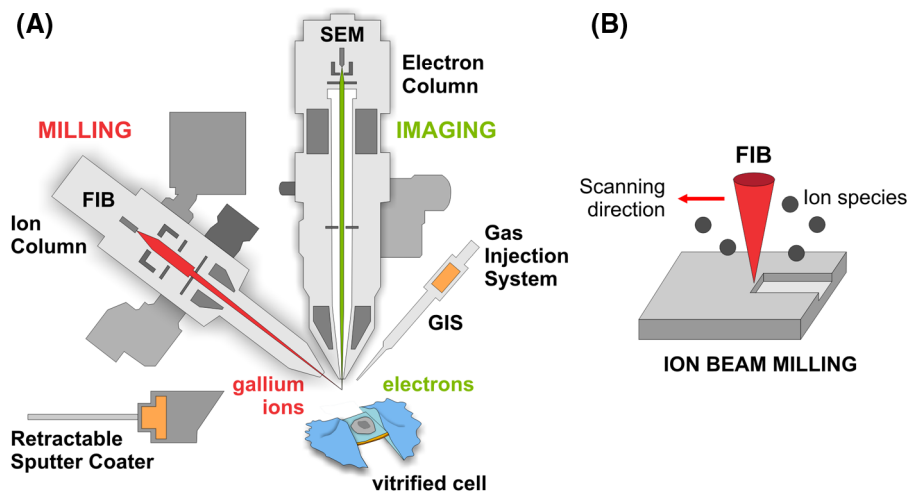


Fig. 3. Operating principle of a cryo-FIB/SEM. All steps relevant for lamella production can be carried out within one instrument. (A) The gallium ion beam is produced by a liquid metal ion source at the top of the ion column. The beam is focused onto the vitrified sample by a set of electrostatic lenses and deflection coils. The electron beam is used to select target regions and monitor the milling process. An integrated sputter coater is used to deposit thin conductive layers of platinum. A gas injection system (GIS) is used prior to milling to apply a thick protective platinum coating onto the vitrified sample, which prevents beam erosion during cryo-lamella production. (B) Principle of ion beam milling. During FIB milling, a focused beam of gallium ions is raster scanned across the sample surface and removes atoms via ion beam sputtering processes.

transfer step between cryo-LM and cryo-FIB, which involves physical manipulation with a tweezer and loss of sample alignment. With the cartridge holder, the sample can be directly transferred after cryo-LM imaging into the FIB-shuttle. The latter is part of the cryo-transfer system that has been designed for the Thermo Scientific Aquilos 2 Cryo-FIB. Since the sample remains in position during the imaging process in both devices, extra manipulation and re-alignment steps become obsolete.

Challenges in high-accuracy targeting

One of the major tasks within the cryo-ET workflow is the high-accuracy targeting of lamella regions based on cryo-LM data. While the targeting in x , y -direction can be done reasonably reliable (Schorb & Briggs, 2014; Ader & Kukulski, 2017; Hampton *et al.*, 2017; Schorb *et al.*, 2017), the critical step is the proper positioning of the milling patterns along the z -axis, such that the target structure visualised in the cryo-light microscope is contained within the resulting lamella. Cryo-lamellae are typically not more than 200 nm thin and neither a commercial widefield microscope nor a confocal microscope alone can achieve a resolution that permits precise z -targeting under cryo-conditions (Fig. 6). Partly this is due to the lack of cryo-immersion objectives, which would allow higher numerical apertures providing a higher resolution. However, superresolution fluorescence microscopy techniques are basically capable to overcome such resolution limitations. Unfortunately, their application under cryo-conditions is still at an early stage with a few proof-of-concept studies available (Chang *et al.*, 2014; Kaufmann *et al.*, 2014; Liu *et al.*, 2015;

Wolff *et al.*, 2016; Moser *et al.*, 2019; Tuijtel *et al.*, 2019). Prominent challenges concern the stability of the system, as long camera exposure times are needed, as well as potential devitrification of the sample. Some systems resolve these issues, yet no commercial solution is available. Currently, approaches based on fiducial correlation techniques are most promising and versatile for achieving the required targeting accuracies (Kukulski *et al.*, 2011; Schellenberger *et al.*, 2014; Arnold *et al.*, 2016; Schorb & Sieckmann, 2017; Fokkema *et al.*, 2018; van Hest *et al.*, 2019). The basic concept involves beads that are visible in both imaging modalities (cryo-LM and cryo-FIB/SEM), which are added to the specimen. Based on exact fitting of the centre coordinates of these beads (by centroid fitting algorithms), the image transformation can be calculated (size, shift and rotation) and the milling patterns can be placed with high accuracy. Open source software for such a 3D correlation is available, providing access to this technique for the scientific community (Arnold *et al.*, 2016; <https://3dct.semper.space>). In combination with a cryo-confocal microscope, this seems to be the method of choice for targeting lamella positions with the currently best achievable accuracy.

New developments extending the application range of the Cryo-FIB

Cryo-FIB sample preparation has developed considerably in recent years since its advent in 2006 (Marko *et al.*, 2006). The method has proven successful in the preparation of vitrified cells for cryo-EM and is currently in high demand in the field of cryo-electron tomography (Rigort & Plitzko, 2015; Nievergelt *et al.*, 2019). As an enabling technology, cryo-FIB is constantly

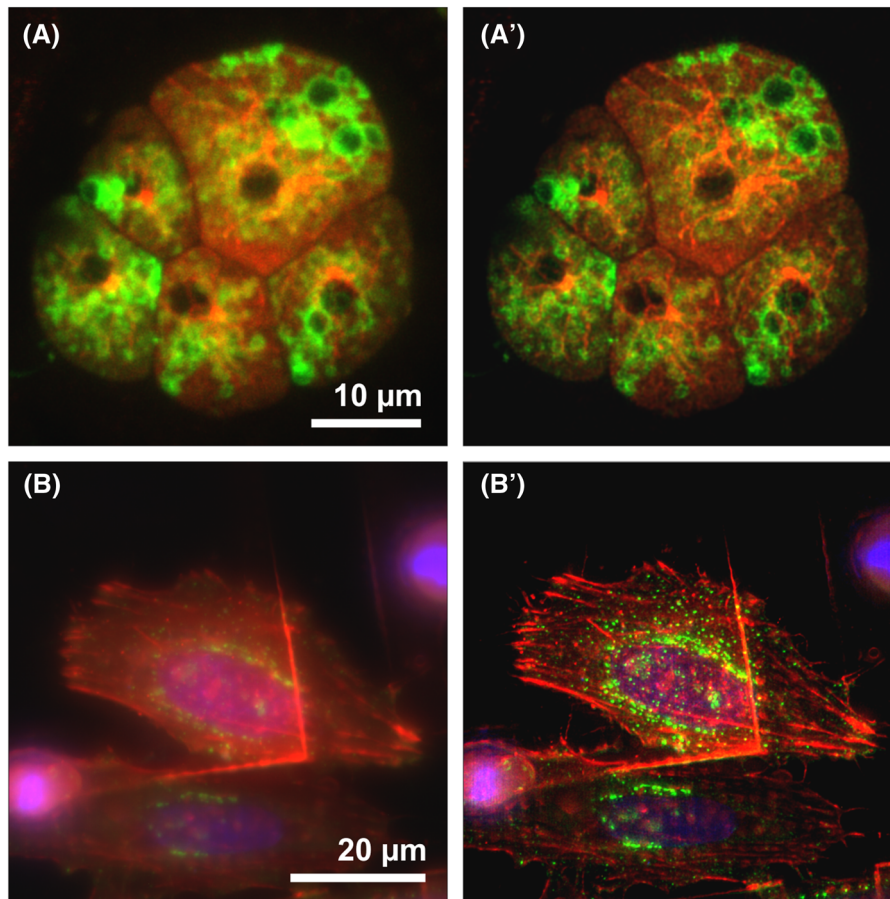


Fig. 4. Comparison between standard and computationally cleared cryo-LM images. (A) Two-channel maximum intensity projection of a z-stack of cryo-confocal images. Sample: *D. discoideum*, green channel: GFP-VatM, red channel: mCherry-Tubulin. (A') The same projection after application of the LIGHTNING computational clearing technology to increase the image quality and resolution. (B) Widefield fluorescence image showing typical haze effect caused by out-of-focus light contributing to the final image. Sample: HeLa cells grown on a Quantifoil grid, red channel: mCherry-F-actin, green channel: GFP-TGN46, blue channel: Hoechst 33342-DNA. Sample courtesy of Dr. Marie-Charlotte Domart & Dr. Lucy Collinson, The Francis Crick Institute, London UK. (B') The same image after haze-removal and increase of signal to noise ratio by computational clearing using THUNDER technology.

being improved and developed further. Below, we introduce three new features we have developed to streamline the use of the cryo-FIB technique and extending its applicability to other fields of application.

Automation software for multi-site lamellae preparation

Automation is a big lever to gain efficiency and improve the milling process of multiple preselected target sites, since the production of several lamellae requires many repetitive steps (Buckley *et al.*, 2020; Zachs *et al.*, 2020). We have therefore developed a dedicated software – called AutoTEM Cryo – for automating lamellae preparation. AutoTEM Cryo runs on the Aquilos 2 Cryo-FIB and is an application which allows users setting up multi-site milling experiments within a graphical user interface. The software allows users to first select the respective milling sites and save their positions (Fig. 7). Afterwards, adjustments to the milling settings can be made, such

as customising shape factors of the milling patterns to match the selected target cells, as well as the definition of milling times and currents. The pattern geometry and placement can be adjusted as desired and several steps can be selected for coarse and fine milling. Once the selection of target sites for milling is finished and patterning parameters have been defined, a list displays the number of milling sites with their consecutive processing times and the total time of the automated milling run. After confirmation by the user, the automated sample run can be started. It is common practice to set up the run in such a way, that all lamellae sites are first roughly milled and only then the final polishing steps are carried out. This is done to minimise the effects of contamination and re-deposition from ion sputtering. During automated milling, AutoTEM Cryo monitors the placement of the patterns and performs drift corrections. This allows the stable and reproducible preparation of lamellae from multiple sites. Lamellae are automatically thinned down to 200 nm thickness, which allows

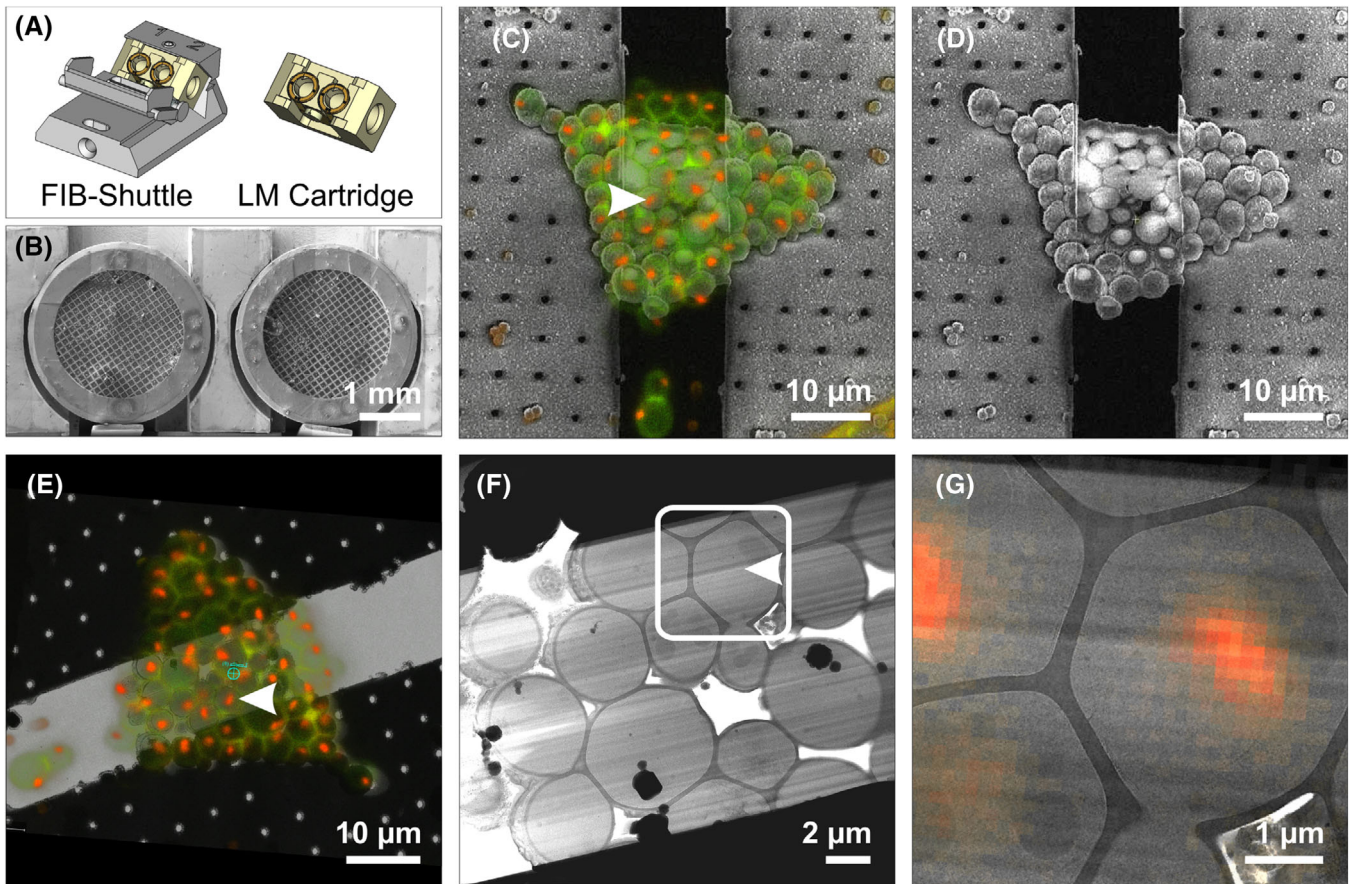


Fig. 5. Correlative targeting example utilising the new cryo-CLEM developments. (A) Dual-use cryo-FIB shuttle and cryo-LM cartridge. (B) SEM overview image of the cryo-LM cartridge with two mounted autogrids. (C) Widefield cryo-fluorescence image of a cluster of *S. cerevisiae* cells (green channel: autofluorescence of the cell wall, red channel: nucleolus marker NOP56) correlated to the cryo-SEM image during lamella preparation (white arrowhead marks the target cell). (D) Corresponding SEM image only. (E) Cryo-TEM image of the final lamella overlaid with the cryo-fluorescence image from (E). (F) The same lamella at higher magnification. White arrowheads in (E) and (F) point to the target cell. (G) Magnified region from the inset in (F) showing the correlation of the cryo-LM image with the lamella. The red nucleolar marker is clearly visible in the targeted cell.

to transfer them after the sample job is finished immediately to the cryo-TEM for electron tomography (Fig. 7C). The number of milling sites which can be defined in AutoTEM Cryo is not limited. However, it needs to be considered that the final polishing steps cannot be carried out for all lamellae at the same time and that a certain amount of material redeposits on the cleaned surfaces as other surfaces are being polished (in particular when the milling sites are close together and only one mesh (60–130 μm) apart). Hence a balance between the total amount of lamellae produced and the level of their cleanliness needs to be found. Figure 8 shows an example of an automated sample run yielding 24 different lamella sites on a single grid. Setting up these milling sites in AutoTEM Cryo took approx. 60 min. The autonomous processing of all 24 sites was carried out within 12 h, taking on average 25–30 min per site. AutoTEM Cryo allows the user to fully customise the milling patterns. This includes for example adding so-called micro-expansion joints (Wolff *et al.*, 2019) to the sides of a lamella

(Figs. 8B–D). These side-cuts can serve as physical buffers to safely absorb material motion and decrease the risk for bending of lamellae.

Cryo-volume imaging for visually approaching target regions within a lamella

Cryo-volume imaging using Auto Slice and View (ASV) software adopts a method that is already well known for 3D imaging of resin embedded biological samples: FIB/SEM tomography (Heymann *et al.*, 2006). The method works by sequentially removing frozen material with the ion beam and imaging the newly created cross-section surfaces with the electron beam to obtain 3D data. Unlike resin-embedded samples treated with heavy metal contrasting agents and imaged with the backscattered electron (BSE) detector, acquisition of non-stained cryo-block faces is only performed by secondary electron (SE) detection. The first reports of this type of SE

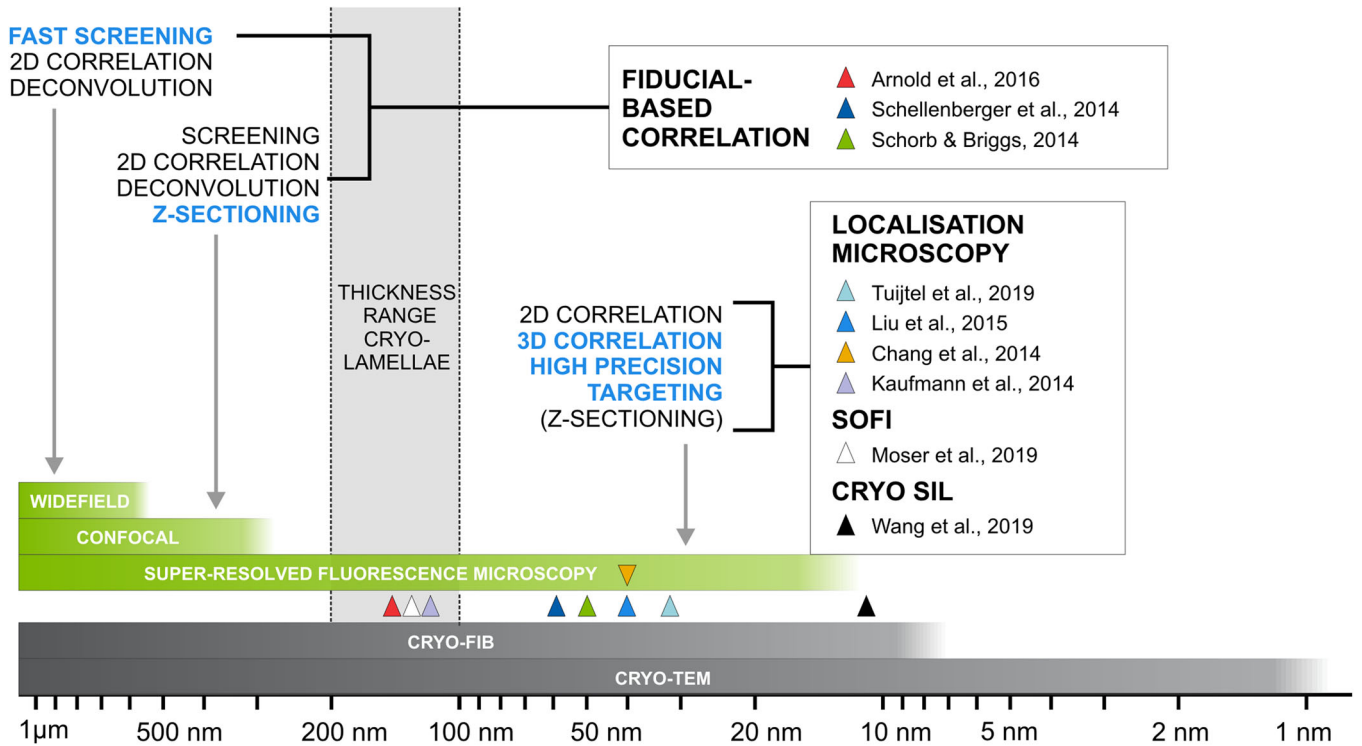


Fig. 6. Overview of the current landscape for cryo-LM with respect to targeting accuracy for lamella preparation. Major advantage of each method highlighted in blue. Neither widefield nor confocal microscopy systems alone are sufficient to achieve the localisation accuracy required to precisely target cellular features within a 200 nm lamella. This is in part due to the lack of cryo-immersion objectives, which would allow higher numerical apertures. Fiducial-based correlation techniques or superresolved microscopy techniques can assist in achieving higher targeting accuracies. One study reported the use of a solid immersion lens (SIL) under cryo-conditions (Wang *et al.*, 2019). Horizontal bars indicate the achievable resolution for each imaging technique.

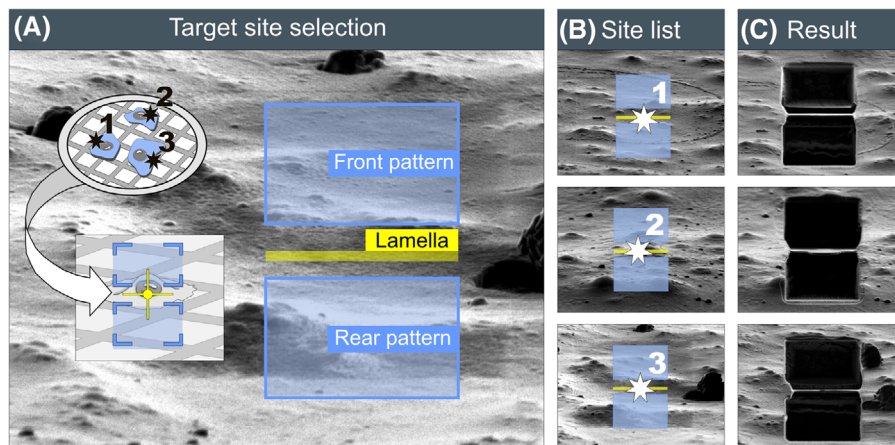


Fig. 7. Lamella milling automation. (A) Schematic illustration showing the principle of selecting multiple cells for an automated milling experiment. (B) Three milling sites are selected. (C) Final result of the automated milling experiment using AutoTEM Cryo software. Three 200 nm lamellae have been produced automatically.

cryo-contrast date back several years (Hayles *et al.*, 2007; Rigort *et al.*, 2010), while the first study showing 3D acquisition was reported in 2013 (Schertel *et al.*, 2013). Figure 9 shows a result obtained by cryo-ASV SE volume imaging of a frozen-

hydrated *Chlamydomonas reinhardtii* cell. The volume of the flash-frozen unicellular green alga visualised in Figure 9(A) is about 150 μm³ and exposes five Golgi complexes, parts of the flagella shaft and nucleus with nucleolus. A cross-section

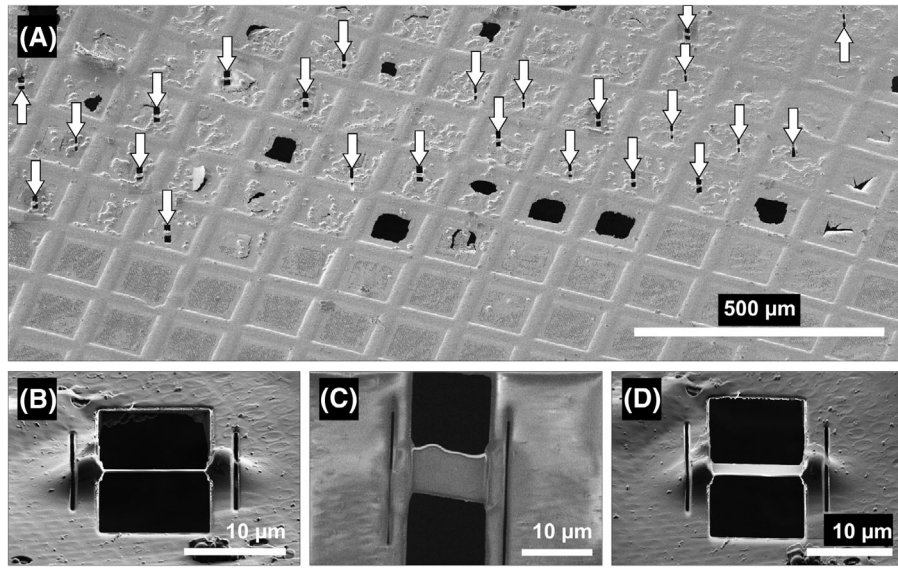


Fig. 8. Automated multi-site lamella preparation. (A) Autonomous milling of 24 cryo-lamellae sites (white arrows) on an EM grid. The milling sites have been set up using AutoTEM Cryo software. The first pass of the automation run is the rough milling of the 24 positions. This is followed by the final polishing run and thinning of the sites to the final thickness of 200 nm. (B)–(D) Detailed side, top and oblique views of a lamella produced by automated milling. Within AutoTEM Cryo, also micro-expansion joints (Wolff *et al.*, 2019) can be defined and processed for each location. Modified with permission from Tacke *et al.* (2020).

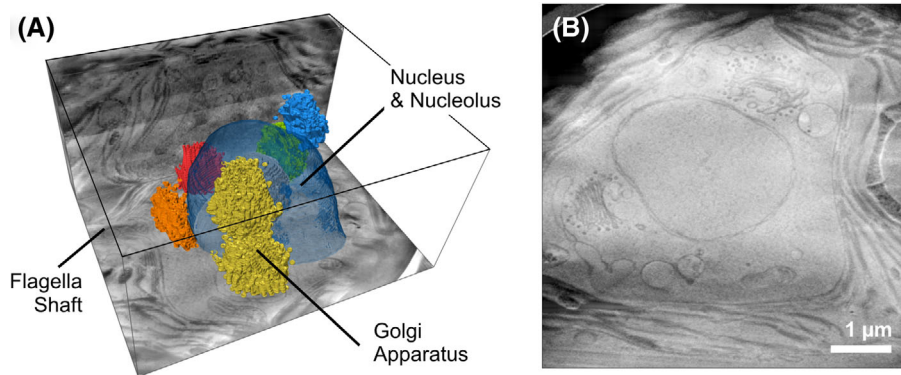


Fig. 9. Cryo-volume imaging using Auto Slice and View (ASV) software. (A) 3D visualisation of a data set obtained by cryo-ASV imaging of a frozen *Chlamydomonas* cell. The volume shown covers approximately $150 \mu\text{m}^3$ of vitrified cellular space. Various Golgi compartments as well as the Nucleus (with Nucleolus inside) are highlighted by 3D segmentation. (B) Top view SE image showing a cross-section from the centre of the 3D stack. The contrast originates from imaging local charge distributions and allows to discern subcellular morphology. Within the nuclear envelope nuclear pores are discernable.

SE image from the centre of this 3D cryo-ASV data set clearly visualises subcellular structures. Clearly discernible in these serial images are the Golgi complexes and associated transport vesicles, the nuclear envelope with nuclear pore complexes, chloroplast thylakoid membranes, mitochondria and endoplasmic reticulum (Fig. 9B and Movies SM1, SM2). Each cross-section was imaged by detection of SE signals with the Everhart–Thornley Detector (ETD) and in-lens detectors. SEM imaging was performed at 2.5 kV, using a probe current of 25 pA. Scanning was done with a 4 nm pixel size and a dwell

time of 100 ns (using $100\times$ line-integration mode). Cryo-ASV imaging can be used to analyse samples that cannot be dehydrated, but it is also advantageous for cryo-lamella preparation. While under visual control by the SEM, top down milling is used across the respective target region step by step until the desired feature or marker becomes visible (e.g. a specific cell organelle in the SE image). Subsequently, the sample can then be thinned further from the back side to the required thickness for TEM tomography (see also the following section on cryo-lift-out).

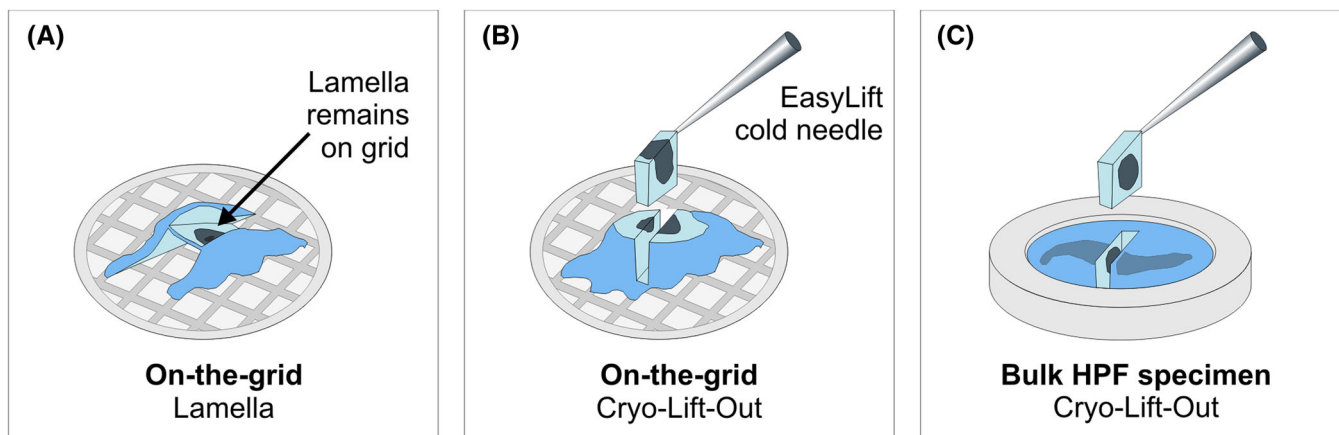


Fig. 10. Lamella preparation approaches for cryo-EM. (A) On-the-grid *in situ* lamella fabrication. The lamella is supported on two sides by the frozen sample and does not require lift-out. The whole grid containing such an 'on-the-grid' lamella is transferred to the TEM for cryo-tomography. (B) On-the-grid cryo-lift-out of a cellular sample and (C) from a bulk HPF frozen sample within an HPF planchette. In both cases the lamella is lifted out and attached to a cooled half-moon lift-out grid, which is clipped into a regular autogrid. Cryo-tomography is then performed using this autogrid.

The cryo-ASV imaging process can start immediately after the sample is frozen and transferred into the cryo-FIB/SEM microscope. Although the resolution of this technique is modest compared to TEM, much larger volumes can be investigated. This allows analysing cellular morphology beyond the 200 nm thickness of a cryo-lamella. However, the contrast formation by secondary electrons in the frozen hydrated block face (see Fig. 9) is still not fully understood. The SE imaging properties are most likely based on charge contrast, where the local surface potential strongly influences the amount of detected secondary electrons. Furthermore, prolonged electron beam irradiation causes beam-induced sublimation, which becomes visible after repeated scanning of the frozen surfaces. In addition, locally confined beam damage effects cannot be ruled out due to the heterogeneous composition of the biological sample. Since the imaging method is based on local surface potential, non-uniform and stochastic charge distributions can occur depending on the sample properties, which can aggravate the imaging process. Also, aspects of beam-sample interactions, such as the depth of the interaction volume and the contribution to the available total electron dose for tomography, must be considered for subsequent lamella preparation.

Cryo-lift-out

Cryo-lift-out is required when the standard 'on-the-grid' lamella preparation (Rigort *et al.*, 2012; Schaffer *et al.*, 2017) is no longer sufficient (Fig. 10A). This can be the case when high-pressure frozen bulk samples need to be processed and where a considerable amount of frozen material must be removed or where the sample is simply not suited for 'on-the-grid' lamella geometries (i.e. where the lamella stays on the grid for electron tomography). Two different use cases are possible for cryo-lift-out applications (Figs. 10B–C). On the one

hand, vitrified samples can be processed directly on the grid with cryo-lift-out. This allows, for example, the preparation of apical sample areas that cannot be targeted using 'on-the-grid' lamella preparation. On the other hand, larger samples frozen in high-pressure freezing (HPF) sample carriers (3 mm planchettes) can now be processed. This is necessary, for example, for accessing frozen cell samples such as tissue biopsies or small organisms. So far, only a few cryo-lift-out applications have been reported (Rubino *et al.*, 2012; Mahamid *et al.*, 2015; Parmenter *et al.*, 2016; Zachman *et al.*, 2016). A recent study successfully combined correlative imaging with site-specific cryo-lift-out and electron tomography at molecular resolution (Schaffer *et al.*, 2019). Current lift-out applications are based on either using a microgripper system (i.e. a nanometre precise tweezer) or needle-based micromanipulators. An advantage of the needle-based systems is the interchangeability of the tungsten needles and the relatively low cost for exchanging the needles compared to the microgripper system.

We have developed a cryo-lift-out system based on the Thermo Fisher Scientific EasyLift Nanomanipulator installed on the Aquilos 2 Cryo-FIB. The use of this system for performing 'on-the-grid' cryo-lift-out is depicted in Figure 11. A target cell on the grid is selected and rendered conductive (Figs. 11A–B) using the Aquilos in-chamber sputter coating system (compare Figs. 2, 3). The target area for the lift-out must be sufficiently large, because the actual thinning of the sample takes place later, after the lift-out has been carried out. Therefore, first a coarse sample is prepared by sputtering material away with the ion beam. This leaves behind a μm thick coarse lamella that is still connected to the surrounding frozen material via two small side bridges (Figs. 11B–C). Next, the cold (-165°C at the tip) tungsten needle of the EasyLift system is brought close to the sample site. The process can be precisely controlled via software integrated in the operating

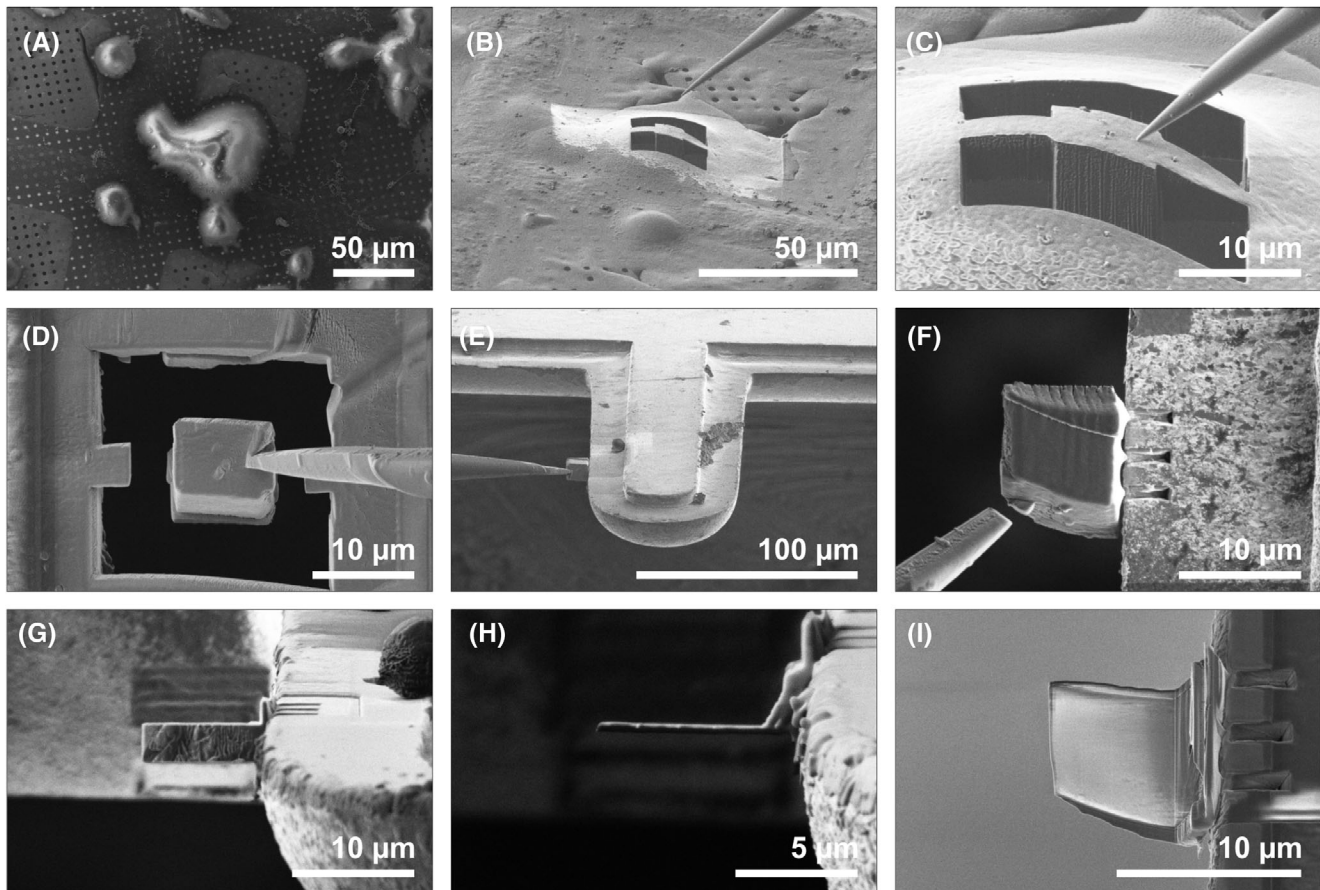


Fig. 11. On-the-grid cryo-lift-out procedure. (A) Vitrified cells. (B) Milling of a chunk for lift-out. (C) Attaching the EasyLift to the coarse lamella by cold Pt deposition. (D) Cutting the coarse lamella. (E) Attaching the coarse lamella to the post of a half-moon grid. (F) Cutting the needle free. (G) Thinning the coarse lamella. (H) Final thinned cryo-lift-out lamella. (I) Top view of cryo-lamella.

system environment. For the needle-to-sample approach, the cold needle is carefully placed onto the coarse lamella. Now a connection between the needle and the frozen sample must be established. Beam-assisted welding procedures, known from room temperature applications (Langford *et al.*, 2001; Langford & Clinton, 2004), cannot be used under cryo-conditions. Instead, cold deposition (Hayles *et al.*, 2007) of the organometallic platinum precursor is used to establish the needle-to-sample contact. After the needle is firmly attached, the coarse lamella is cut free and lifted upwards and away from the cutout region (Fig. 11D). The lamella is then brought to a second autogrid position (within the same cryo-FIB shuttle/sample holder). Mounted in this position is a pre-clipped FIB lift-out grid ('half-moon grid') containing posts for cryo-lamellae attachment. The EasyLift cryo-lift-out system enables lamella attachment directly into an autogrid, eliminating an extra clipping step that can lead to the loss of the fragile lamella. The coarse lamella is positioned in close contact to the post (Fig. 11E). Then milling patterns are applied in such a way that sputtered material from the post redeposits on the lateral side of the coarse lamella (the

method resembles a spot-welding process). This creates a firm connection between the coarse lamella and the half-moon grid post. Once the coarse lamella is firmly attached to the post, the lift-out needle is cut free (Fig. 11F) and moved to a safe parking position. The coarse lamella is then thinned further down to 200 nm using the ion beam under flat angle geometries to achieve TEM transparency. (Figs. 11G–I). The ion beam currents used here correspond to those used for the 'on-the-grid' lamella thinning approach.

As mentioned in the previous section, SE signals obtained by cryo-ASV can be used for guiding the lamella thinning process. Figure 12(A) shows a cryo-lift-out lamella prepared from a high-pressure frozen mouse brain sample. The preparation followed the procedure described above, with the exception that a different sample carrier was used for excavating part of the neuronal tissue. Here, a 3 mm HPF planchette holder has been used (compare Fig. 10C) from which the coarse lamella has been prepared. The charge contrast-based SE image clearly exhibits neuronal morphology. Image filtering (using FFT, local contrast enhancement and non-local means filters in Thermo Scientific Amira software) highlights subcellular

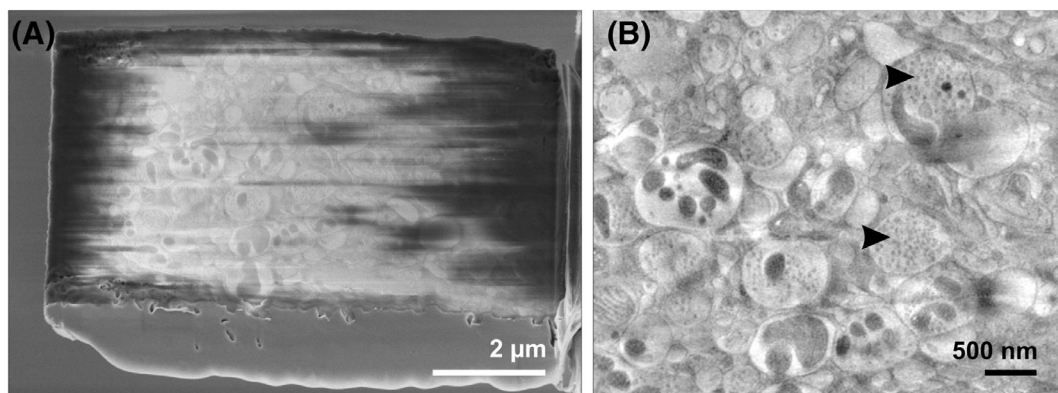


Fig. 12. Bulk HPF sample cryo-lift-out lamella. (A) Cryo-ASV image of a cryo-lift-out lamella from a non-stained high-pressure frozen mouse brain sample. The SE image can be used to screen the neuronal tissue for regions of interest. (B) Magnified region from the centre of the lamella shown in (A). The filtered image clearly shows synaptic vesicles within various neuronal cells (black arrowheads pointing to those vesicles where the lumens of synaptic vesicles can be discerned). Thinning of such a lamella from the back allows end pointing of regions of interest for tomography experiments.

features, such as synaptic vesicles in the magnified image from the central lamella region. The SE imaging resolution permits seeing the lumens of some of the synaptic vesicles (Fig. 12B, arrowheads). Cryo-ASV can be used here, to localise synaptic regions for example. The lamella can then be thinned down from its back side to the thickness required to yield the TEM transparency. Using such a ‘back-thinning’ approach can facilitate the identification and targeted preparation of synaptic areas for cryo-ET analysis.

Challenges and perspectives

The primary objective of the entire cryo-tomography workflow is to obtain reliable, reproducible and site-specific 3D data. In order to get there, still several challenges need to be overcome. The precise and specific localisation of target sites remains a major challenge in the workflow. Here, better software integration and the dual-use shuttle described above can provide some remedy by allowing the workflow to become more connected and reproducible. The implementation of cryo-ASV can add an additional level of correlative information (by introducing an extra imaging modality beside cryo-LM) and thus also contribute to faster localisation of targets. Software-driven automation approaches, as presented here, allow to increase the throughput of lamellae production and can increase the yield of utilisable lamellae for cryo-tomography. Finally, cryo-lift-out allows the use of other milling geometries than those possible for *in situ* on-the-grid lamella preparation. This provides access to previously inaccessible sample areas and allows the processing of HPF samples. The challenge for the future will be improving the connection between the individual workflow steps and to greatly reduce manual manipulation steps. Manual manipulation steps carry the risk of damaging the sample, changing its orientation or introducing unwanted contamination. Severe transfer contamination, for example, by tiny

ice crystals obstructing the field of view can prevent that any subsequent workflow steps can be carried out. Also, ice build-up rates during transfers and within the cryo-FIB and cryo-TEM instruments must be strictly controlled, as they directly influence the achievable image quality and contrast during tomography. Any developments aimed at eliminating potential sources of contamination will therefore be in great demand. Much of the current progress in cryo-tomography is already owed to the technical innovations in sample preparation made possible by dedicated cryo-dual beam microscopes. With these instruments it is now possible to look inside the frozen-hydrated interior of a cell more routinely. We believe that the cryo-FIB technique will continue to be transformative for the field of cryo-tomography.

Acknowledgements

We would like to acknowledge Sebastian Tacke (Max Planck Institute of Molecular Physiology) and Sven Klumpe (Max Planck Institute of Biochemistry) for beta-testing AutoTEM Cryo. JK and MH would like to acknowledge the Laboratory of Electron Microscopy, Institute of Parasitology, Biology Centre CAS, supported by the MEYS CR (LM2015062 Czech-BioImaging), for their support with HPF sample preparation. We would like to further thank Robert Brandt and Tilman Franke for their support in processing cryo-ASV images in Amira and Radim Kříž and Matěj Dolník for developing AutoTEM Cryo software. AR would like to thank Mary Ecke and Günther Gerisch for providing samples and Wolfgang Baumeister and Jürgen Plitzko for their support.

References

- Ader, N.R. & Kukulski, W. (2017) triCLEM: combining high-precision, room temperature CLEM with cryo-fluorescence microscopy to identify very rare events. *Methods Cell Biol.* **140**, 303–320.

- Albert, S., Wietrzynski, W., Lee, C.W. *et al.* (2020) Direct visualization of degradation microcompartments at the ER membrane. *Proc. Natl. Acad. Sci. U.S.A.* **117**(2), 1069–1080.
- Arnold, J., Mahamid, J., Lucic, V. *et al.* (2016) Site-specific cryo-focused ion beam sample preparation guided by 3D correlative microscopy. *Biophys. J.* **110**(4), 860–9.
- Briegleb, A., Chen, S., Koster, A.J., Plitzko, J.M., Schwartz, C.L. & Jensen, G.J. (2010) Correlated light and electron cryo-microscopy. *Methods Enzymol.* **481**, 317–341.
- Brüggeller, P. & Mayer, E. (1980) Complete vitrification in pure liquid water and dilute aqueous solutions. *Nature* **288**(5791), 569–571.
- Buckley, G., Gervinkas, G., Taveneau, C., Venugopal, H., Whisstock, J.C. & de Marco, A. (2020) Automated cryo-lamella preparation for high-throughput in-situ structural biology. *J. Struct. Biol.* **210**, 107488.
- Chang, Y.W., Chen, S., Tocheva, E.I. *et al.* (2014) Correlated cryogenic photoactivated localization microscopy and cryo-electron tomography. *Nat. Methods* **11**(7), 737–739.
- Dubochet, J., Adrian, M., Chang, J.J. *et al.* (1988) Cryo-electron microscopy of vitrified specimens. *Q. Rev. Biophys.* **21**(2), 129–228.
- Dubochet, J. & McDowell, A.W. (1981) Vitrification of pure water for electron microscopy. *J. Microsc.* **124**(3), 3–4.
- Faas, F.G., Barcena, M., Agronskaia, A.V. *et al.* (2013) Localization of fluorescently labeled structures in frozen-hydrated samples using integrated light electron microscopy. *J. Struct. Biol.* **181**(3), 283–290.
- Faoro, R., Bassu, M., Mejia, Y.X. *et al.* (2018) Aberration-corrected cryo-immersion light microscopy. *Proc. Natl. Acad. Sci. U.S.A.* **115**(6), 1204–1209.
- Fokkema, J., Fermie, J., Liv, N. *et al.* (2018) Fluorescently labelled silica coated gold nanoparticles as fiducial markers for correlative light and electron microscopy. *Sci. Rep.* **8**(1), 13625.
- Gorelick, S., Buckley, G., Gervinkas, G. *et al.* (2019) PIE-scope, integrated cryo-correlative light and FIB/SEM microscopy. *Elife* **8**, e45919. <https://doi.org/10.7554/eLife.45919>.
- Guo, Q., Lehmer, C., Martinez-Sanchez, A. *et al.* (2018) In Situ structure of neuronal C9orf72 Poly-GA aggregates reveals proteasome recruitment. *Cell* **172**(4), 696–705 e12.
- Hampton, C.M., Strauss, J.D., Ke, Z. *et al.* (2017) Correlated fluorescence microscopy and cryo-electron tomography of virus-infected or transfected mammalian cells. *Nat. Protoc.* **12**(1), 150–167.
- Hayles, M.E., Stokes, D.J., Phifer, D. & Findlay, K.C. (2007) A technique for improved focused ion beam milling of cryo-prepared life science specimens. *J. Microsc.* **226**(Pt 3), 263–269.
- Heymann, J.A., Hayles, M., Gestmann, I., Giannuzzi, L.A., Lich, B. & Subramaniam, S. (2006) Site-specific 3D imaging of cells and tissues with a dual beam microscope. *J. Struct. Biol.* **155**(1), 63–73.
- Kaufmann, R., Hagen, C. & Grunewald, K. (2014) Fluorescence cryo-microscopy: current challenges and prospects. *Curr. Opin. Chem. Biol.* **20**, 86–91.
- Kaufmann, R., Schellenberger, P., Seiradake, E. *et al.* (2014) Super-resolution microscopy using standard fluorescent proteins in intact cells under cryo-conditions. *Nano Lett.* **14**(7), 4171–4175.
- Koning, R.I., Celler, K., Willemsse, J., Bos, E., van Wezel, G.P. & Koster, A.J. (2014) Correlative cryo-fluorescence light microscopy and cryo-electron tomography of *Streptomyces*. *Methods Cell Biol.* **124**, 217–239.
- Kukulski, W., Schorb, M., Welsch, S., Picco, A., Kaksonen, M. & Briggs, J.A. (2011) Correlated fluorescence and 3D electron microscopy with high sensitivity and spatial precision. *J. Cell. Biol.* **192**(1), 111–119.
- Langford, R.M. & Clinton, C. (2004) In situ lift-out using a FIB-SEM system. *Micron* **35**(7), 607–611.
- Langford, R.M., Huang, Y.Z., Lozano-Perez, S., Titchmarsh, J.M. & Petford-Long, A.K. (2001) Preparation of site specific transmission electron microscopy plan-view specimens using a focused ion beam system. *J. Vacuum Sci. Technol. B: Microelectr. Nanometer Struct. Process., Measure., Phenom.* **19**(3), 755–758.
- Le Gros, M.A., McDermott, G., Uchida, M., Knoechel, C.G. & Larabell, C.A. (2009) High-aperture cryogenic light microscopy. *J. Microsc.* **235**(1), 1–8.
- Liu, B., Xue, Y., Zhao, W. *et al.* (2015) Three-dimensional super-resolution protein localization correlated with vitrified cellular context. *Sci. Rep.* **5**, 13017.
- Mahamid, J., Pfeffer, S., Schaffer, M. *et al.* (2016) Visualizing the molecular sociology at the HeLa cell nuclear periphery. *Science* **351**(6276), 969–672.
- Mahamid, J., Schampers, R., Persoon, H., Hyman, A.A., Baumeister, W. & Plitzko, J.M. (2015) A focused ion beam milling and lift-out approach for site-specific preparation of frozen-hydrated lamellas from multicellular organisms. *J. Struct. Biol.* **192**(2), 262–269.
- Marko, M., Hsieh, C., Moberlychan, W., Mannella, C.A. & Frank, J. (2006) Focused ion beam milling of vitreous water: prospects for an alternative to cryo-ultramicrotomy of frozen-hydrated biological samples. *J. Microsc.* **222**(Pt 1), 42–47.
- Marko, M., Hsieh, C., Schalek, R., Frank, J. & Mannella, C. (2007) Focused ion-beam thinning of frozen-hydrated biological specimens for cryo-electron microscopy. *Nat. Methods* **4**(3), 215–217.
- Mosalaganti, S., Kosinski, J., Albert, S. *et al.* (2018) In situ architecture of the algal nuclear pore complex. *Nat. Commun.* **9**(1), 2361.
- Moser, E., Prazak, V., Mordhorst, V. *et al.* (2019) Cryo-SOFI enabling low-dose super-resolution correlative light and electron cryo-microscopy. *Proc. Natl. Acad. Sci. U.S.A.* **116**(11), 4804–4809.
- Nahmani, M., Lanahan, C., DeRosier, D. & Turrigiano, G.G. (2017) High-numerical-aperture cryogenic light microscopy for increased precision of superresolution reconstructions. *Proc. Natl. Acad. Sci. U.S.A.* **114**(15), 3832–3836.
- Nievergelt, A.P., Viar, G.A. & Pigino, G. (2019) Towards a mechanistic understanding of cellular processes by cryoEM. *Curr. Opin. Struct. Biol.* **58**, 149–158.
- Parmenter, C.D., Fay, M.W., Hartfield, C. & Eltaher, H.M. (2016) Making the practically impossible “Merely difficult” – Cryogenic FIB lift-out for “Damage free” soft matter imaging. *Microsc. Res. Tech.* **79**(4), 298–303.
- Plitzko, J. & Baumeister, W.P. (2019) Cryo-electron tomography. *Springer Handbook of Microscopy* (ed. by P.W. Hawkes & J.C.H. Spence), p. 2. Springer International Publishing, Cham.
- Reymann, J. (2018) Lightning – Image Information Extraction by Adaptive Deconvolution. Leica Microsystems White Paper. 1–13. https://downloads.leica-microsystems.com/LIGHTNING/Publications/LIGHTNING_Whitepaper_v_Mar2020.pdf.
- Rigort, A., Bauerlein, F.J., Leis, A. *et al.* (2010) Micromachining tools and correlative approaches for cellular cryo-electron tomography. *J. Struct. Biol.* **172**(2), 169–179.
- Rigort, A., Bauerlein, F.J., Villa, E. *et al.* (2012) Focused ion beam micromachining of eukaryotic cells for cryoelectron tomography. *Proc. Natl. Acad. Sci. U.S.A.* **109**(12), 4449–4454.
- Rigort, A. & Plitzko, J.M. (2015) Cryo-focused-ion-beam applications in structural biology. *Arch. Biochem. Biophys.* **581**, 122–130.

- Rubino, S., Akhtar, S., Melin, P., Searle, A., Spellward, P. & Leifer, K. (2012) A site-specific focused-ion-beam lift-out method for cryo Transmission Electron Microscopy. *J. Struct. Biol.* **180**(3), 572–576.
- Sartori, A., Gatz, R., Beck, F., Rigort, A., Baumeister, W. & Plitzko, J.M. (2007) Correlative microscopy: bridging the gap between fluorescence light microscopy and cryo-electron tomography. *J. Struct. Biol.* **160**(2), 135–145.
- Schaffer, M., Engel, B.D., Laugks, T., Mahamid, J., Plitzko, J.M. & Baumeister, W. (2015) Cryo-focused ion beam sample preparation for imaging vitreous cells by cryo-electron tomography. *Bio. Protoc.* **5**(17), e1575.
- Schaffer, M., Mahamid, J., Engel, B.D., Laugks, T., Baumeister, W. & Plitzko, J.M. (2017) Optimized cryo-focused ion beam sample preparation aimed at in situ structural studies of membrane proteins. *J. Struct. Biol.* **197**(2), 73–82.
- Schaffer, M., Pfeffer, S., Mahamid, J. *et al.* (2019) A cryo-FIB lift-out technique enables molecular-resolution cryo-ET within native *Caenorhabditis elegans* tissue. *Nat. Methods* **16**(8), 757–762.
- Schellenberger, P., Kaufmann, R., Siebert, C.A., Hagen, C., Wodrich, H. & Grunewald, K. (2014) High-precision correlative fluorescence and electron cryo microscopy using two independent alignment markers. *Ultramicroscopy* **143**, 41–51.
- Schertel, A., Snaidero, N., Han, H.M. *et al.* (2013) Cryo FIB-SEM: volume imaging of cellular ultrastructure in native frozen specimens. *J. Struct. Biol.* **184**(2), 355–360.
- Schorb, M. & Briggs, J.A. (2014) Correlated cryo-fluorescence and cryo-electron microscopy with high spatial precision and improved sensitivity. *Ultramicroscopy* **143**, 24–32.
- Schorb, M., Gaechter, L., Avinoam, O. *et al.* (2017) New hardware and workflows for semi-automated correlative cryo-fluorescence and cryo-electron microscopy/tomography. *J. Struct. Biol.* **197**(2), 83–93.
- Schorb, M. & Sieckmann, E. (2017) Matrix MAPS – an intuitive software to acquire, analyze, and annotate light microscopy data for CLEM. *Methods Cell Biol.* **140**, 321–333.
- Schumacher, J. & Bertrand, L. (2019) THUNDER Imagers: How Do They Really Work? Leica Microsystems Technology Note. 1–10. www.leica-microsystems.com/science-lab/thunder-technology-note/.
- Schwartz, C.L., Sarbash, V.I., Ataullakhanov, F.I., McIntosh, J.R. & Nicastro, D. (2007) Cryo-fluorescence microscopy facilitates correlations between light and cryo-electron microscopy and reduces the rate of photobleaching. *J. Microsc.* **227**(Pt 2), 98–109.
- Tacke, S., Erdmann, P., Wang, Z. *et al.* (2020) A streamlined workflow for automated cryo focused ion beam milling. *bioRxiv*. <https://doi.org/10.1101/2020.02.24.96303>.
- Tuijtel, M.W., Koster, A.J., Jakobs, S., Faas, E.G.A. & Sharp, T.H. (2019) Correlative cryo super-resolution light and electron microscopy on mammalian cells using fluorescent proteins. *Sci. Rep.* **9**(1), 1369.
- van Driel, L.F., Valentijn, J.A., Valentijn, K.M., Koning, R.I. & Koster, A.J. (2009) Tools for correlative cryo-fluorescence microscopy and cryo-electron tomography applied to whole mitochondria in human endothelial cells. *Eur. J. Cell Biol.* **88**(11), 669–684.
- van Hest, J.J.H.A., Agronskaia, A.V., Fokkema, J. *et al.* (2019) Towards robust and versatile single nanoparticle fiducial markers for correlative light and electron microscopy. *J. Microsc.* **274**(1), 13–22.
- Wagner, J., Schaffer, M. & Fernandez-Busnadiego, R. (2017) Cryo-electron tomography – the cell biology that came in from the cold. *FEBS Lett.* **591**(17), 2520–2533.
- Wan, W. & Briggs, J.A. (2016) Cryo-electron tomography and subtomogram averaging. *Methods Enzymol.* **579**, 329–367.
- Wang, L., Bateman, B., Zanetti-Domingues, L.C. *et al.* (2019) Solid immersion microscopy images cells under cryogenic conditions with 12 nm resolution. *Commun. Biol.* **2**, 74.
- Wolff, G., Hagen, C., Grunewald, K. & Kaufmann, R. (2016) Towards correlative super-resolution fluorescence and electron cryo-microscopy. *Biol. Cell* **108**(9), 245–258.
- Wolff, G., Limpens, R., Zheng, S. *et al.* (2019) Mind the gap: micro-expansion joints drastically decrease the bending of FIB-milled cryo-lamellae. *J. Struct. Biol.* **208**(3), 107389.
- Zachman, M.J., Asenath-Smith, E., Estroff, L.A. & Kourkoutis, L.F. (2016) Site-specific preparation of intact solid-liquid interfaces by label-free in situ localization and cryo-focused ion beam lift-Out. *Microsc. Microanal.* **22**(6), 1338–1349.
- Zachs, T., Schertel, A., Medeiros, J. *et al.* (2020) Fully automated, sequential focused ion beam milling for cryo-electron tomography. *Elife* **9**, e52286. <https://doi.org/10.7554/eLife.52286>.
- Zhang, P. (2019) Advances in cryo-electron tomography and subtomogram averaging and classification. *Curr. Opin. Struct. Biol.* **58**, 249–258.

Supporting Information

Additional supporting information may be found online in the Supporting Information section at the end of the article.

Movie SM1. Movie showing the 3D visualisation of the cryo-ASV data from Figure 9(A). 3D visualisation created with the Thermo Scientific Amira software.

Movie SM2. Movie corresponding to Figure 9(B) showing cross-sectioning through the volume that has been obtained by cryo-ASV imaging.